Graded-reflectance mirrors for beam quality control in laser resonators

G. Duplain, P. G. Verly, J. A. Dobrowolski, A. Waldorf, and S. Bussière

Several types of small-dimension graded-reflectance mirrors deposited through rotating masks are compared. Multilayer mirrors provided with single-variable-thickness layers have limitations that are avoided when all the layers in the system are shaped. High-reflectance mirrors of the latter type are demonstrated. Numerical and experimental results are given.

1. Introduction

Over two decades ago theoretical studies indicated that soft apertures or variable-reflectance mirrors reduce the detrimental effects of edge diffraction in optical resonators.[1–6] A number of different approaches have been proposed in the past for the implementation of this principle.[7] Of these, the use of graded-reflectance mirrors (GRM's), also known as variable-reflectance mirrors has proved to be the most practical.

Since the first experimental demonstration of a GRM based on a variable-thickness nonabsorbing layer by Lavigne *et al.*,[8] a number of other papers have been published that confirm this principle.[9–17] The use of GRM's is now a commercially accepted means of producing high-energy single-transverse-mode laser beams with unstable resonators operating on high-gain media. Such beams have uniform intracavity near-field distributions, and an almost diffraction-limited far-field pattern.

In a typical laser resonator the GRM is the output coupler, and it has a circularly symmetric reflectance profile. The variation of the reflectance R with radius r can assume almost any value, but most frequently it obeys a Gaussian ($k = 2$) or super-Gaussian ($k > 2$) relation of the type

$$R(r) = R_0 \exp[-(r/\omega)^k].$$

Here R_0 is the on-axis (or peak) reflectance and ω is the waist or radius vector at which the reflectance is reduced to $1/e$ of its peak value. Examples of Gaussian and super-Gaussian curves are given in Fig. 1.

Several multilayer types and masking techniques can be used for the manufacture of GRM's. Lavigne *et al.*[8] deposited a single-variable-thickness layer through a mask onto an antireflection-coasted (AR) substrate. This is the simplest or basic GRM type. Higher peak reflectances require additional layers. In the sandwich GRM type one or more shaped layers is embedded in a stack of layers of uniform thicknesses.[14,15] In the fully shaped GRM type all the layers have variable thicknesses.[16,17]

The masks can be fixed or rotating. The latter offer a better control of the radial-reflectance variations but they are more difficult to fabricate. In this study we show that the deposition of GRM's through rotating masks is an effective technique, even when the mask dimensions are quite small.

The three types of GRM are described in greater detail in Sections 2–4. The advantages and disadvantages of stationary and rotating masks are discussed in Section 5. Section 6 contains a description of the vacuum-coating equipment and process. Section 7 is concerned with the testing and evaluation of the experimental coatings. Finally the results are summarized in Section 8.

2. GRM's of the Basic Type

As we mentioned in Section 1, the simplest way to produce a GRM is to deposit a single high-refractive-index layer through a suitably cut mask. The substrate must be transparent and must have been coated previously with a uniform antireflection coating.[8] A schematic representation of such a device is shown in Fig. 2A. Major laser manufacturers are now offering GRM's of this type for use in Nd:YAG and similar lasers.

G. Duplain and S. Bussière are with the National Optics Institute, 369 rue Franquet (C.P.9970), Sainte-Foy (Quebec City), Quebec G1V 4C5, Canada. The other authors are with the National Research Council of Canada, Ottawa, Ontario K1A 0R6, Canada.

Received 13 February 1992.

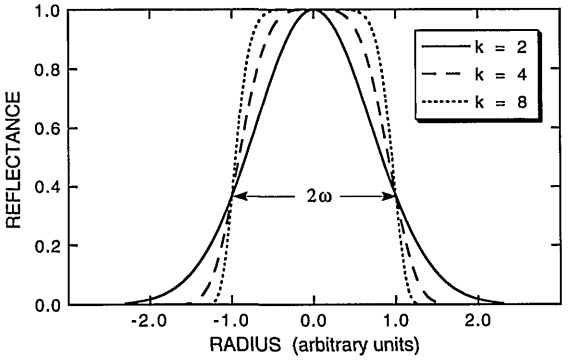

Fig. 1. Reflectance versus radius curves for Gaussian ($k = 2$) and super-Gaussian ($k > 2$) GRM's (see text).

The reflectance at the design wavelength λ_0 decreases from a peak value of R_0 at $r = 0$ to a minimum at the edge of the GRM where the thickness of the shaped layer is zero. At that point the reflectance corresponds to that of the AR substrate. Between these two limits the required reflectance profile is obtained through a suitable shaping of the mask. The maximum value of R_0 is achieved when the optical thickness of the shaped layer is equal to $\lambda_0/4$ and its refractive index n has the highest possible value. This in turn depends on the spectral region and, for laser applications, on the minimum acceptable laser damage threshold. For example, reflectances of the order of 75% are possible at CO_2 laser wavelengths ($\lambda_0 \approx 10.6$ μm) at which thin films of germanium ($n = 4.2$) are transparent.[8] In the UV, visible, and near-IR spectral regions the highest refractive indices available for high-laser-damage-threshold coatings are of the order of 2.1. This limits R_0 to ~40%. Coatings for low-power lasers can be based on materials with slightly higher refractive indices.

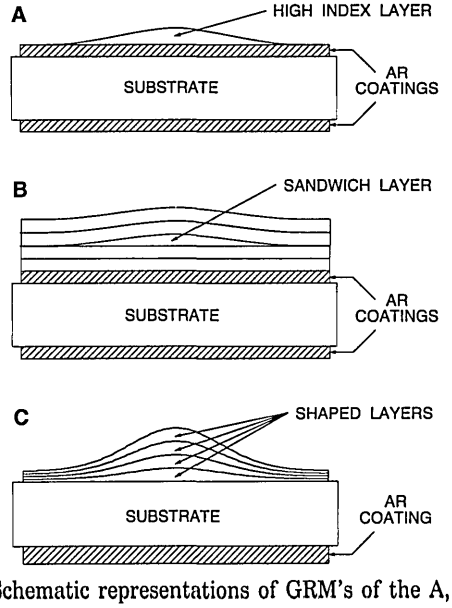

Fig. 2. Schematic representations of GRM's of the A, basic; B, sandwich; and C, fully shaped types.

Calculated results for a Gaussian GRM of small dimensions are shown in Fig. 3. This example was chosen to illustrate the effect of mask-fabrication limitations on the performance. The wavelength of operation is the YAG laser wavelength $\lambda_0 = 1.064$ μm, and the coating materials are SiO_2 ($n = 1.44$) and ZrO_2 ($n = 2.03$). All the systems presented in this paper are based on these materials or on SiO_2 and Ta_2O_5 ($n = 2.2$). The shape of the required mask is shown in Fig. 3A. The open portion is narrow, and the tips, which ideally should end in sharp points, have been rounded. They have a diameter of 0.3 mm to simulate the limitations of our mask-fabrication technique. This truncation results in a distortion of the thickness and reflectance profiles (Figs. 3B and 3C). The phase jumps in Fig. 3D have a different origin and occur at slightly different radial positions. The maximum reflectance possible with this design is relatively small, $R_{max} = 0.37$. The calculations have been performed for normal incidence.

The radial optical path variations in GRM's distort the reflected and transmitted wave fronts. This may result in diffraction, focusing, hot spots, etc., which are detrimental to the operation of a laser. The reflection phase shifts are particularly important because they affect the light properties within the laser resonator. Figure 3D shows the radial variation of the reflection phase shift calculated in plane P, relative to the central value (see the inset in Fig. 3D). This represents also the phase-front deformation of an incident plane wave after reflection. It will be seen that the phase variation is small, except for a sharp discontinuity of $\sim\pi/5$ (or $\lambda_0/10$) at the edge of the GRM. From experience it appears that variations of this magnitude do not unduly affect the

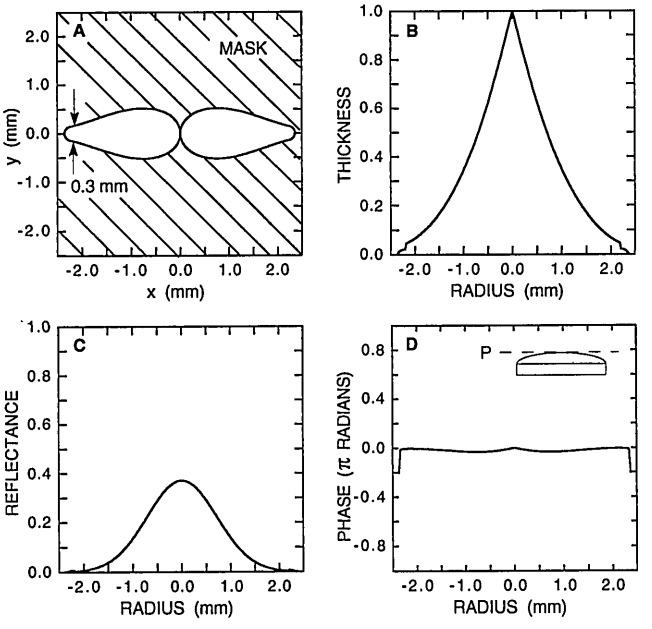

Fig. 3. A, calculated mask profile; B, C, thickness and reflectance variations; D, distortion of the reflected phase front for a Gaussian GRM of the basic type with $\lambda_0 = 1.064$ μm, $R_0 = 0.37$, and $\omega = 1$ mm.

performance of lasers.[13] This is especially true if the energy in the region of the phase jump is small.

The calculated and measured reflectance profiles of an experimentally produced GRM of extremely small dimensions (ω = 0.78 mm) are shown in Fig. 4. It is quite interesting that such small GRM's can be fabricated with such good precision. The equipment and procedures used for the deposition and testing of the GRM's are described in Sections 5–8.

3. GRM's of the Sandwich Type

For higher reflectances more layers must be employed. In GRM's of the sandwich type the shaped layer is embedded in a stack of layers of uniform thickness. Such systems have been proposed in the past, but to our knowledge practical results have not been described in detail.[14,15,17]

Our implementation of the concept is shown in Fig. 2B. Here the graded layer is sandwiched between two quarter-wave stacks that are mirror images of one another. When the optical thickness nt of the shaped layer is also equal to $\lambda_0/4$, the combined system acts like a quarter-wave stack and the reflectance is a maximum. We can fine tune the peak reference of the GRM by varying t. At the edge of the GRM $t = 0$, and the remaining layers in the quarter-wave stack become absentee. Once again the reflectance of the system is equal to the reflectance of the AR-coated substrate. The shape of the mask is adjusted so that we obtain the desired reflectance profile between these two extreme positions.

Variants of this concept are possible. For example, the use of the quarter-wave stacks is not essential, several layers can be graded, their position in the stack can be varied, and their thicknesses do not have to be reduced to zero at the edge of the mirror. We chose the GRM geometry shown in Fig. 2B because it is simple and capable of high peak reflectances and low edge reflectances with a minimum number of layers.

However, these GRM's have some limitations. Because only one layer is shaped, the mask must be inserted and removed in the middle of the coating process. Three separate pump-down cycles are needed. This is inconvenient, increases the risk of contamination and scatter, and can affect the laser damage threshold of the mirrors. Note that the problem is the same with all the other sandwich variants. There are some additional difficulties in the case of high reflectances. At the edge of the GRM, where the quarter-wave stack is absentee, the spectral characteristics of the system correspond to those of a narrow-band filter. Such a system is quite sensitive to errors in thicknesses, and achieving a zero reflectance will therefore be difficult. The problem can be expected to be even more severe for systems with more than one shaped layer, which behave in the AR region like higher-order or multicavity narrow-band filters.[17] Finally masks for GRM's of small dimensions become increasingly difficult to produce as the reflectance increases.

The points above are illustrated by two examples. The first of these is a successful super-Gaussian GRM (k = 3) for λ_0 = 0.810 μm with R_0 = 0.84 and ω = 3.3 mm. The multilayer consists of a two-layer AR coating and a five-layer reflector (Fig. 5A). The shaped layer is indicated by an arrow. The required mask is shown in Fig. 5B. It has a relatively large aperture and can be produced with good accuracy. Note that the tips of the mask are again rounded with the same radius as before. The calculated super-Gaussian reflectance profile and the deformation of the reflected phase are shown in Figs. 5C and 5D, respectively. The latter has an amplitude of $\sim\pi/5$, if the phase jump in the AR region is excluded. This is larger than in the previous example but still small enough for most applications. A GRM according to

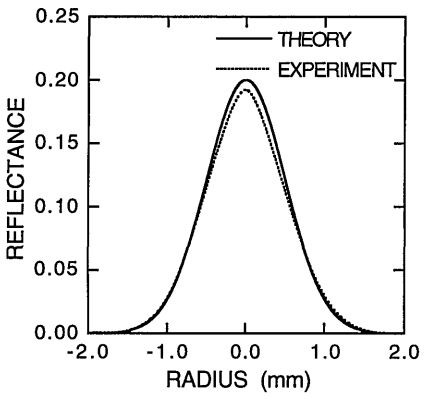

Fig. 4. Theoretical and experimental results for a Gaussian GRM of the basic type with λ_0 = 1.064 μm, R_0 = 0.20, and ω = 0.78 mm.

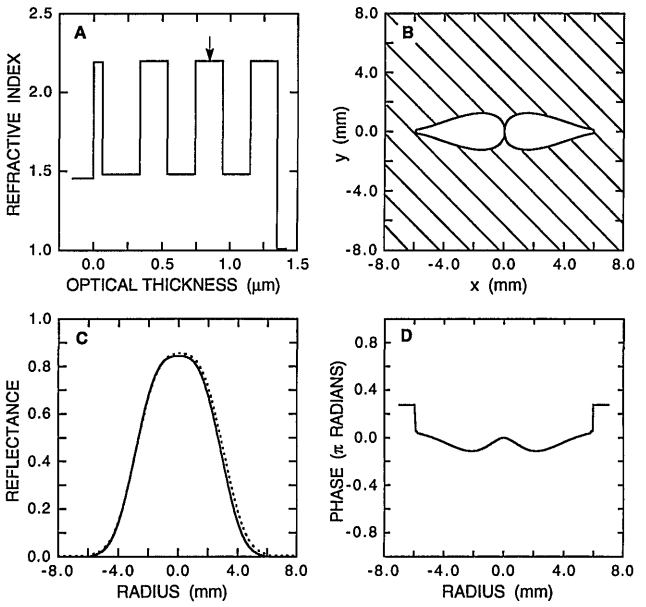

Fig. 5. A, B, refractive index and mask profiles; C, calculated reflectance variation; D, distortion of the reflected phase front for a super-Gaussian (k = 3) GRM of the sandwich type with λ_0 = 0.810 μm, R_0 = 0.84, and ω = 3.3 mm. The shaped layer is indicated by an arrow in A. The dotted curve in C corresponds to experimental measurements.

the above specifications has been produced. The measured reflection profile is represented by the dotted curve in Fig. 5C. The agreement between the calculated and experimental data is quite good.

The next calculations correspond to a GRM that was found to be too difficult to implement in practice (Fig. 6). The maximum reflectance, $R_0 = 0.85$, was specified for a wavelength of $\lambda_0 = 1.064$ μm. However, this time the reflectance profile was Gaussian ($k = 2$) and the waist was only $\omega = 1.0$ mm. A multilayer system similar to the previous one with a satisfactory reflectance profile and a phase variation has been found (Figs. 6A, 6C, and 6D). Unfortunately the width of the mask aperture barely exceeded the resolution of our mask-fabrication technique (Fig. 6B). Such a mask would be too difficult to make with sufficient accuracy. In general it has been found that as the value of k decreases and that of R_0 increases, the y/x aspect ratio of the mask opening decreases, making the fabrication of small masks more difficult. This can be seen by comparing Figs. 3, 5, and 6.

4. Fully Shaped GRM Systems

A third GRM type based on the use of fully shaped multilayer systems is illustrated in Fig. 2C. All the layers are deposited through the same mask, and hence their relative thickness variations are the same. The deposition process is now continuous, without the need of venting of the chamber for the introduction or removal of masks. This shortens the manufacturing time and reduces contamination.

GRM's of this type have been proposed in the past. In Ref. 16 the coatings were deposited through fixed masks. With this technique the variation in thickness is due to the shadow effect, and there is only a limited control of the reflectance profile (see Section 5). The consequences are particularly serious in the present case. Since all the layer thicknesses are zero in the shadow of the mask, the substrate cannot be antireflection coated in this region. Furthermore the large thickness variations tend to create undesired sidelobes in the reflectance curve unless the system consists of only a few layers; in which case the peak reflectance is relatively low.[14]

The deposition of fully shaped GRM's through rotating masks does not have the same limitations. We also found that it has some additional advantages over the other approaches described in the previous sections. This technique was proposed in Ref. 17, but practical results were not described in detail.

With fully shaped GRM's we optimized both the layer thicknesses and the mask shape to achieve the desired performance. The system is designed to be a good reflector at $r = 0$ and an antireflection coating at the edge of the GRM. In general the thicknesses of all the layers will be different. The additional degrees of freedom that now exist can be used to find thin-film solutions that are less sensitive to thickness errors and that work in conjunction with masks that are easier to produce. For example, it is possible to reduce the problems that are associated with the sensitivity to thickness errors in the region of low reflectance.

In Fig. 7 are shown the calculated results for a fully shaped GRM with exactly the same specifications as those used in Fig. 6. The new system consists of nine layers (Fig. 7A). Note the almost symmetrical chirp of the layer thicknesses. The reflectance profile is the same as before (Figs. 6C and 7C), but the

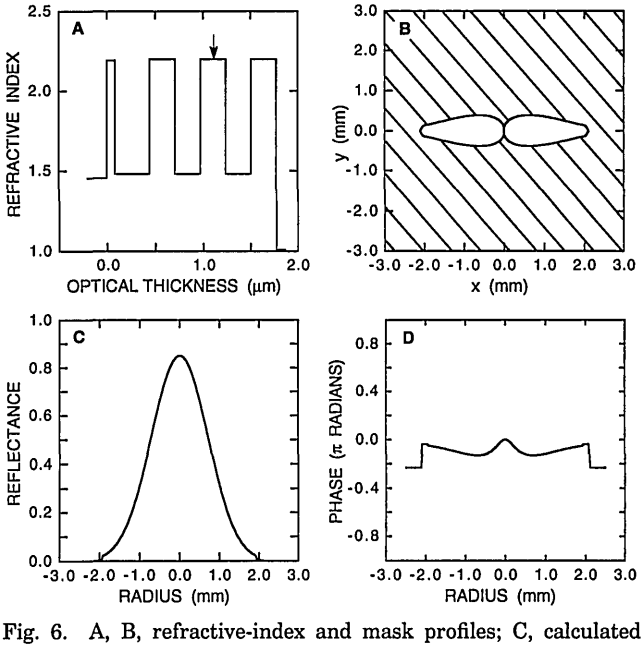

Fig. 6. A, B, refractive-index and mask profiles; C, calculated reflectance variation; D, distortion of the reflected phase front for a Gaussian GRM of the sandwich type with $\lambda_0 = 1.064$ μm, $R_0 = 0.85$, and $\omega = 1.0$ mm.

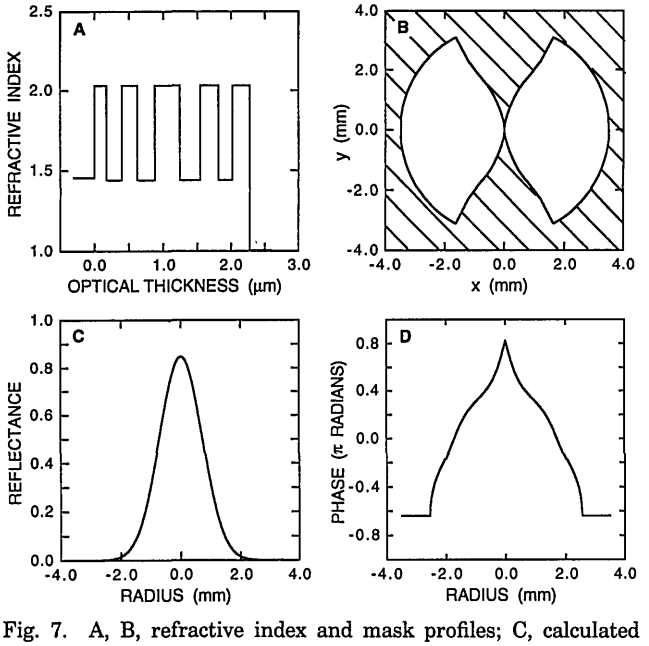

Fig. 7. A, B, refractive index and mask profiles; C, calculated reflectance variation; D, distortion of the reflected phase front for a fully shaped Gaussian GRM with $\lambda_0 = 1.064$ μm, $R_0 = 0.85$, and $\omega = 1.0$ mm.

mask opening is now much larger (Fig. 7B). This is because the thicknesses of the layers at the edge of the GRM have finite values. The mask fabrication is therefore easier. One disadvantage of this solution is that the distortion of the reflected phase fronts is larger (Fig. 7D). This is due to the fact that all the layers are shaped. Even if the thickness variation in each layer were smaller than before, the combined overall thickness variation of the multilayer is larger. The resulting phase variation may be too large for some applications.

Preliminary experimental results for a fully shaped super-Gaussian ($k = 4$) GRM with a small waist $\omega = 1.9$ mm and a maximum reflectance $R_0 = 0.85$ at a wavelength of $\lambda_0 = 1.064$ μm are shown in Fig. 8. The measured peak reflectance was only ~0.8. According to numerical simulations, this and the small irregularities near the peak are probably a result of thickness errors. The AR region appears to have a low sensitivity to such errors since a reflectance of 0.0007 in the AR region was obtained without difficulty.

As stated before the phase variation of the fully shaped GRM shown in Fig. 7D is probably larger than can be accepted for use in most laser resonators. Until now the phase variation was not a design parameter in the calculations. It was merely calculated for the multilayer systems that satisfied the requirements on the reflectance profile. In the case of GRM's of the basic and sandwich types the phase variation was automatically small enough. It is obvious from the above that this is not true in general and that for the design of the fully shaped GRM's phase constraints must also be included in the specifications. The results of some preliminary calculations of this type are shown in Fig. 9. The specifications for this problem were the same as for Fig. 7 except that in addition a constant phase factor was specified. The system consists now of 15 layers. The residual reflectance at the edge of the mirror is very small, the phase variation is also very small, and there is no phase jump. The mask is easy to fabricate. A detailed discussion of such phase-controlled GRM's will be given in another publication.

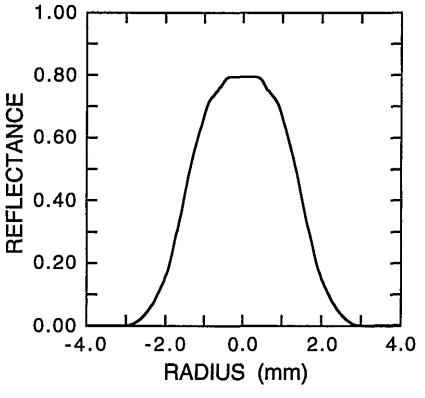

Fig. 8. Experimental result for a super-Gaussian ($k = 4$) fully shaped GRM with $\lambda_0 = 1.064$ μm, $R_0 = 0.85$, and $\omega = 1.9$ mm.

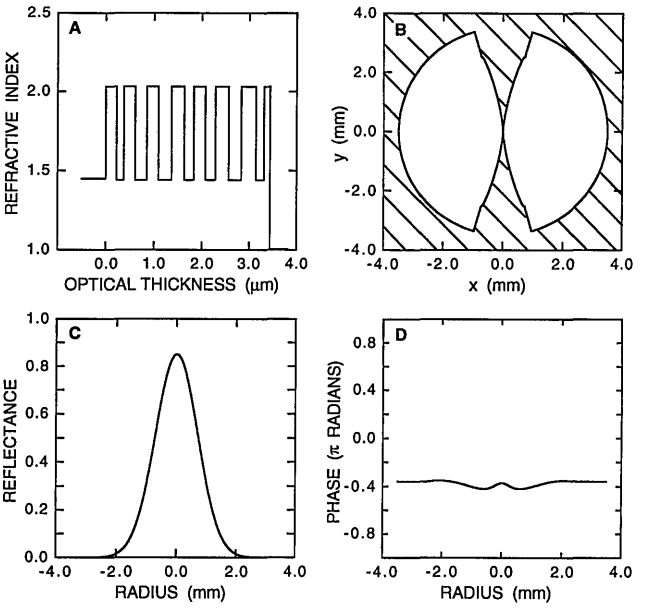

Fig. 9. A, B, refractive-index and mask profiles; C, calculated reflectance variation; D, distortion of the reflected phase front for a fully shaped Gaussian GRM with $\lambda_0 = 1.064$ μm, $R_0 = 0.85$, and $\omega = 1.0$ mm. A zero-phase distortion was specified in these calculations.

5. Masking Operations for Shaped Layer Deposition

Films with thicknesses that vary in a predetermined way can be produced by evaporation through a suitable mask. For example, various optical filters in which the transmittance or reflectance varies along a straight line[18] or along the circumference of a circle have been made.[19,20] It is more pertinent to the current problem that metallic or dielectric films with radial thickness variations have been used to produce aspheric reflecting or refracting surfaces.[21–24] There are four different masking approaches to the fabrication of coatings with such circular symmetry.

A. Stationary Substrate and Mask (Fig. 10A)

In this arrangement the mask has a circular opening of diameter D and is placed at a distance h from the substrate. The evaporation source has a finite diameter d and is centered below the mask at a distance H away from the substrate. The thickness of the deposit is uniform across a central area. The falloff in thickness in the penumbra region depends on the relative dimensions of d, D, h, and H. The arrangement is simple, but there are not enough parameters for accurate control of the variation in thickness. Although this method has been used for the manufacture of some types of GRM, it does not seem to be suitable for super-Gaussian GRM's of low order and large waist or of high order and small waist.[15,16] Additional problems encountered during the manufacture of fully shaped GRM's with stationary mask and subtrate are mentioned in Section 4.

B. Rotating Substrate and Stationary Mask (Fig. 10B)

A suitably cut mask is placed vertically above the source. The substrate is rotated in close proximity

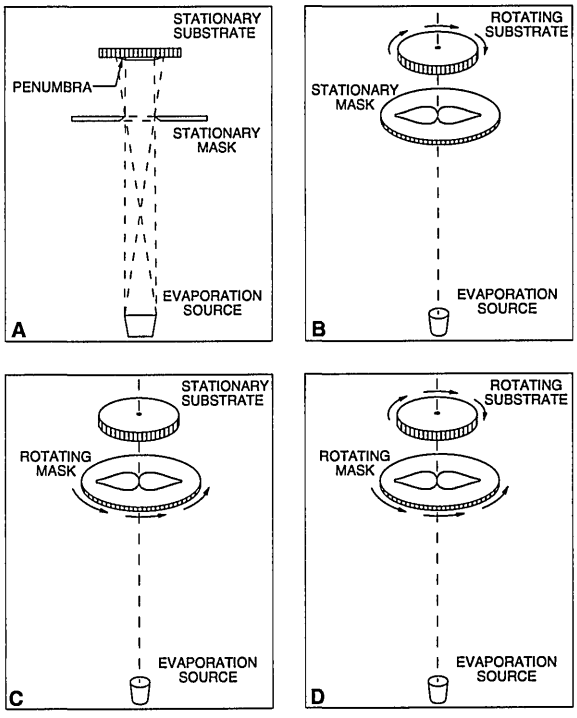

Fig. 10. Mask and substrate arrangements for the deposition of layers with radially varying thicknesses: A, stationary substrate and mask; B, rotating substrate and stationary mask; C, stationary substrate and rotating mask; D, rotating substrate and rotating mask.

to the mask. The rate of rotation is such that many rotations are required for the deposition of the layer. The required angular opening $\theta(r)$ of the mask to yield a film of thickness $t(r)$ is given by the expression

$$\theta(r) = \theta(r_0)t(r)/t_0.$$

Here t_0 is the thickness of the film at the center of the substrate, and $\theta(r)_0$ is a normalization factor. Theoretically this method can produce almost any desired circularly symmetric reflectance profile.

C. Stationary Substrate and Rotating Mask (Fig. 10C)

In principle this approach is equivalent to the method described in Subsection 5.B, and the cut of the mask is evaluated from the same equation.

D. Rotating Substrate and Rotating Mask (Fig. 10D)

In this arrangement the substrate and the mask rotate in opposite directions and the gears driving the two components are chosen so that beats are prevented from occurring during the time required for the deposition of the layer. Once again, we can use the expression given in Subsection 5.B to calculate the opening of the mask.

As already stated, method A does not have the degrees of freedom necessary to control accurately the thickness profile of the layer. In ideal situations in which the angular evaporation characteristics of the source are constant throughout the deposition and the vapor plume has circular symmetry and is aimed at the center of the substrate, each of the remaining three methods yield equivalent results. However, in practice these assumptions are not always justified. For example, the effect of a tilted plume in the case of a rotating substrate above a stationary mask will result in a circularly symmetrical deposit but with distorted thickness profile. In the case of a stationary substrate above a rotating mask the same condition will give rise to an asymmetry in the thickness profile on the substrate, but the average profile will be approximately correct. The use of masks in which the required opening has been distributed in several identical segments can reduce these effects. However, this is at the expense of an added complexity in the mask manufacture and the introduction of more cutting errors. The double rotation (method D) provides for still better averaging but is much more difficult to implement.

It has been found that when sufficient care is exercised, the stationary-substrate rotating-mask method can yield entirely satisfactory results. A computer program has been developed that simulates the expected thickness profile for different masks and source–substrate distances. With the aid of this code the best deposition configuration can be found and the optimum mask shape calculated for a given thickness profile. The masks must then be cut accurately. The fixture that holds the substrate and provides for the rotation of the mask had to be machined to strict tolerances, and it must be regularly maintained. The masks have to be carefully mounted on the rotating fixture if holes or bumps at the center of the GRM are to be avoided. However, with these precautions the equipment and methods described above yielded during the past few years many different reflectance profiles, even of very small dimensions, with a high degree of accuracy. For example, Gaussian and super-Gaussian profiles with values of ω_m as small as 0.6 mm have been accurately produced (Fig. 4).

6. Vacuum-Coating Equipment and Process

Most of the GRM's described in this paper were deposited in a conventional 45-cm-diameter stainless-steel bell-jar system pumped by a 15-cm-diameter diffusion pump. The base pressure of this system, 5×10^{-6} Torr, could be reached after 60 min of pumping with LN_2 in the baffle. A four-crucible electron-beam gun source was used for the evaporation of the coating materials. The materials selected for construction of the mirrors were SiO_2 and ZrO_2 because of their good transparency in the wavelength region of operation (0.81 and 1.064 μm). The starting materials for the SiO_2 layers were fused silica disks. The evaporation took place at a pressure of 1×10^{-5} Torr. The ZrO_2 films were produced by the reactive evaporation of Zircaloy in an oxygen partial pressure of 1×10^{-4} Torr.[25]

Before the deposition the substrates were carefully cleaned in an ultrasonic bath and placed in the rotating mask fixture. The substrate was mounted

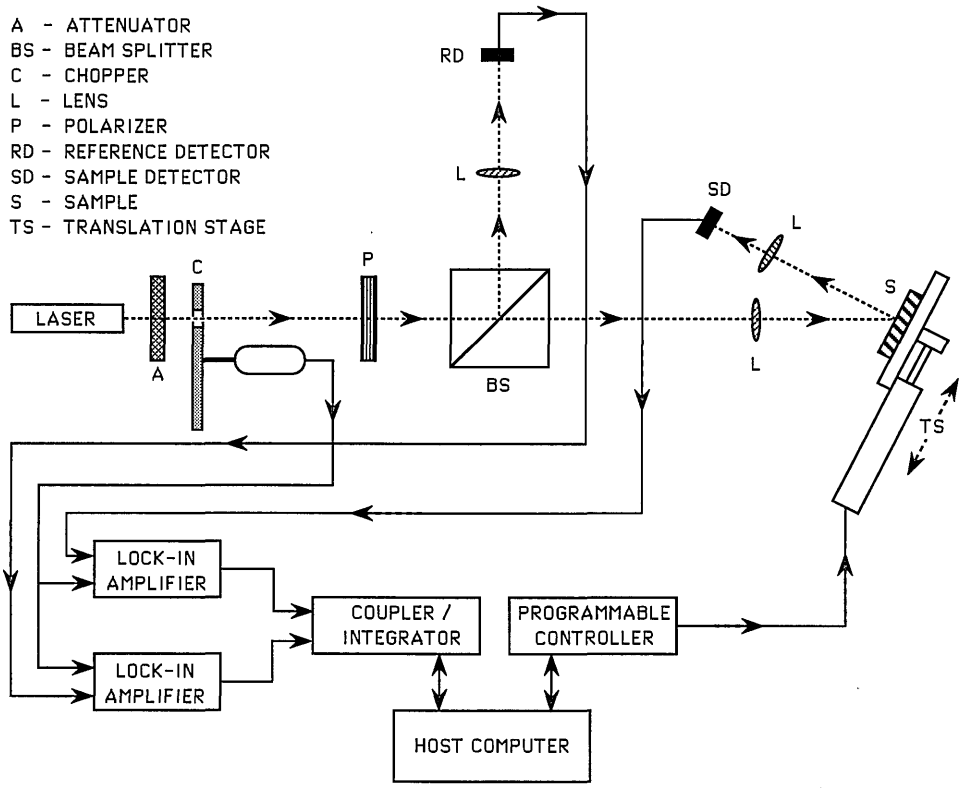

Fig. 11. Schematic diagram of the equipment for the reflectivity profile measurements.

directly above the evaporation source. The optical monitoring was performed on a separate witness glass placed to one side of the substrate. Calibration runs were necessary for determination of the tooling factor. The most sensitive wavelength monitoring method was used to control the thickness of the layers.[26,27] Light from a quartz halogen lamp, after passing through the witness glass, was focused with mirrors and lenses onto the slit of a grating monochromator. For each layer of the system the wavelength of the monochromator was selected to correspond to that position in the spectrum at which the derivative of the transmittance with respect to the layer thickness was largest for the desired thickness of the layer. The signal from the photomultiplier placed at the exit slit of the monochromator was recorded on a plotter. The deposition process was terminated when the measured transmittance corresponded to the calculated transmittance of the partial system up to this point.

Depending on the type of GRM being constructed, all layers or one only were deposited through the mask. In the latter case two or three pump-down sequences were required to complete the deposition of the final system.

The multilayer whose measured performance is presented in Fig. 5 was based on films of SiO_2 and Ta_2O_5 deposited in a Balzers BAP 800 ion-plating system.

7. Testing of GRM's

A schematic diagram of the apparatus used for the measurement of the reflectivity profiles is shown in Fig. 11. A diode-pumped Nd:YAG laser serves as the light source. After the beam is passed through a light chopper and several other optical components, it is focused onto the surface of the GRM. The angle of incidence of the laser beam on the sample is of the order of 4°, and its diameter is of the order of 50 μm. This assures a very high spatial resolution (see Fig. 4).

A ratio method with two beams and two detectors is used for the measurements. Before a reflectivity profile is taken, the system is calibrated with a reflectance standard placed on the translation stage. For example, the reflectance of a freshly cleaned silica surface is used as a standard for measurements of AR surfaces. After the calibration the GRM is mounted on the translation stage, and we obtain a scan of the reflectivity profile by moving the mirror across the beam.

Two lock-in amplifiers and an integrator coupler are used in the measurements. The latter makes possible the real-time calculation of the ratio of the sample and reference signals. The main advantage of using an integrator coupler is the elimination of transient ratio errors as a result of unbalanced time constants of the lock-in amplifiers. With this system it is possible to measure with good reproducibility reflectances that are lower than 0.01%.

8. Conclusions

The rotating-mask technique has been used to fabricate several types of GRM. It was found to be effective even for GRM's of small dimensions.

The simplest GRM designs are those of the basic type, which consists of a single graded thickness layer deposited onto an AR substrate. The peak reflectance that can be achieved in this way is usually quite low, except for that IR part of the spectrum in which low-absorption, extremely high-refractive-index coating materials are available.

Higher reflectances can be achieved with GRM's in which the graded layer is sandwiched between quarter-wave stacks. The performance of these, however, is sensitive in the antireflection region to errors in the thicknesses of the individual layers of the system. In addition the masks are difficult to produce for small-waist low-order super-Gaussian reflectance profiles. With both of the above types of GRM the coating process has to be interrupted for mask installation.

When the mask is used throughout the deposition process, all the layers are shaped. No interruption of the coating process is required. We can optimize both the layer thicknesses and the mask shape to achieve the desired performance. In general the layer thicknesses are all different. We can use the additional degrees of freedom available with this approach to obtain solutions with an improved performance and/or masks that are easier to cut. This was verified experimentally even for narrow-waist high-reflectance Gaussian GRM's that are difficult to obtain with the sandwich technique.

In general the distortion of the phase fronts by such mirrors is greater than for the first two GRM types. However, preliminary calculations have indicates that the reflected phase-front distortion can be reduced to comparable levels by controlling the phase during the design stage (Fig. 12). A more detailed description of these phase-controlled fully shaped GRM's will be given elsewhere.

The authors acknowledge the assistance of Michel Laliberte and Mars Ranger at various stages of the construction of the deposition equipment. They also thank one of the reviewers for bringing to their attention the study described in Ref. 17. A summary of this paper was first presented at the Annual Meeting of the Optical Society of America, November 1991, in San Jose, Calif.

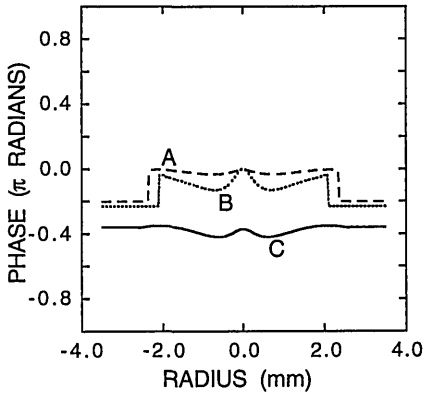

Fig. 12. Comparison of the reflected phase-front distortions for the three GRM types: A, basic; B, sandwich; C, fully shaped, respectively, from Figs. 3, 6, and 9.

References

1. S. N. Vlasov and V. I. Talanov, "Selection of axial modes in open resonators," Radio Eng. Electron. Phys. **10,** 469–470 (1965).
2. N. G. Vahitov, "Open resonators with mirrors having variable reflection coefficients," Radio Eng. Electron. Phys. **10,** 1439–1446 (1965).
3. N. Kumagi, H. Mori, and T. Shiozawa, "Resonant modes in a Fabry–Perot resonator consisting of nonuniform reflectors," Electron. Commun. Jpn. **49,** 1–73 (1966).
4. Y. Suematsu, K. Iga, H. Nagashima, and T. Kitano, "A light beam waveguide using Gaussian-mode filters together with lenses," Electron. Commun. Jpn. **51-B,** 67–74 (1968).
5. H. Zucker, "Optical resonators with variable reflectivity mirrors," Bell Syst. Tech. J. **49,** 2349–2376 (1970).
6. Y. Ananev and V. E. Shertobitov, "Influence of the edge effects on the properties of unstable resonators," Sov. J. Quantum Electron. **1,** 263–267 (1971).
7. P. Lavigne and A. Parent, "Mode control in unstable Cassegrainian resonators," in *Laser Radar II,* R. J. Becherer and R. C. Harneg, eds., Proc. Soc. Photo-Opt. Instrum. Eng. **783,** 69–76 (1987).
8. P. Lavigne, N. McCarthy, and J.-G. Demers, "Design and characterization of complementary Gaussian reflectivity mirrors," Appl. Opt. **24,** 2581–2586 (1985).
9. N. McCarthy, and P. Lavigne, "Large-size Gaussian mode in unstable resonators using Gaussian mirrors," Opt. Lett. **10,** 553–555 (1985).
10. S. D. Silvestri, P. Laporta, V. Magni, O. Svelto, C. Arnone, C. Cali, S. Sciortino, and C. Zizzo, "Nd:YAG laser with multidielectric variable reflectivity output coupler," Opt. Commun. **67,** 229–232 (1988).
11. A. Parent, N. McCarthy, and P. Lavigne, "Effects of hard apertures on mode properties of resonators with Gaussian reflectivity mirrors," IEEE J. Quantum Electron. **QE-23,** 222–228 (1987).
12. A. Caprara, S. Butcher, and R. Aubert, "Injection seeding of a Nd:YAG laser utilizing a radially variable reflectivity output coupler," in *Pulse Single-Frequency Lasers: Technology and Applications,* W. K. Bischel and L. A. Rahn, eds., Proc. Soc. Photo-Opt. Instrum. Eng. **912,** 21–31 (1988).
13. N. McCarthy, P. Lavigne, J.-G. Demers, and A. Parent, "Design and characterization of graded reflectivity mirrors," in *Optical Technology and Metrology,* C. P. Grover, ed., Proc. Soc. Photo-Opt. Instrum. Eng. **661,** 365–371 (1986).
14. A. Piegari, A. Tirabassi, and G. Emiliani, "Thin films for special laser mirrors with radially variable reflectance: production techniques and laser testing," in *Thin Films in Optics,* T. T. Tschudi, ed., Proc. Soc. Photo-Opt. Instrum. Eng. **1125,** 68–73 (1989).
15. G. Emiliani, A. Piegari, S. de Silvestri, P. Laporta, and V. Magni, "Optical coatings with variable reflectance for laser mirrors," Appl. Opt. **28,** 2832–2837 (1989).
16. C. Zizzo, C. Arnone, C. Cali, and S. Sciortino, "Fabrication and characterization of tuned Gaussian mirrors for visible and the near infrared," Opt. Lett. **13,** 342–344 (1988).
17. D. R. Brock, M. J. Taylor, and S. W. Warren, "The design of graded reflectivity mirrors," in *Proceedings of Frontiers in Electrooptics International Conference* (Laser Focus World, Birmingham, UK, 1990), pp. 99–110.
18. J. A. Dobrowolski, G. R. Hanes, and C. J. Van der Hoeven, "Variable interference reflectors with independently settable wavelength and reflectance," Appl. Opt. **7,** 1981–1985 (1968).

19. A. Thelen, "Circularly wedged optical coatings. I. Theory," Appl. Opt. **4,** 977–981 (1965).
20. J. H. Apfel, "Circularly wedged optical coatings. II. Experimental," Appl. Opt. **4,** 983–985 (1965).
21. J. Strong and E. Gaviola, "On the figuring and correcting of mirrors by controlled deposition of aluminum," J. Opt. Soc. Am. **26,** 153–162 (1936).
22. J. A. Dobrowolski and W. Weinstein, "Optical aspherising by vacuum evaporation," Nature (London) **175,** 646–647 (1955).
23. J. R. Kurdock and R. R. Austin, "Correction of optical elements by the addition of evaporated films," in *Physics of Thin Films,* G. Hass and M. H. Francombe, eds. (Academic, New York, 1978), pp. 261–308.
24. J. D. Martin, "Evaporative deposition of aspheric surfaces," M.Sc. thesis (University of Rochester, Rochester, N.Y., 1988).
25. J. A. Dobrowolski, P. D. Grant, R. Simpson, and A. J. Waldorf, "Investigation of the evaporation process conditions on the optical constants of zirconia films," Appl. Opt. **28,** 3997–4005 (1989).
26. J. A. Dobrowolski and A.J. Waldorf, "Manufacture of all-dielectric interference filters of arbitrary thickness and refractive index," J. Opt. Soc. Am. **60,** 725 (A) (1970).
27. J. A. Dobrowolski, "Design and construction of unconventional interference filters," in *Optical Coatings: Applications and Utilization II,* G. W. DeBell and D. H. Harrison, eds., Proc. Soc. Photo-Opt. Instrum. Eng. **140,** 102–108 (1978).